

Article

Preparation and Anti-Corrosive Properties of Waterborne Epoxy Composite Coating Containing Graphene Oxide Grafted with Sodium Tripolyphosphate

Na Wang ^{1,2,3,*}, Xu Yin ¹, Jing Zhang ¹, Huiying Gao ¹, Xinlin Diao ¹ and Hongrui Yao ^{1,*}

¹ Sino-Spanish Advanced Materials Institute, Shenyang University of Chemical Technology, Shenyang 110142, China; 18240119126@163.com (X.Y.); zhangjingcszx@syuct.edu.cn (J.Z.); ghy724@163.com (H.G.); 15702426903@163.com (X.D.)

² Liaoning Provincial Key Laboratory of Rubber & Elastomer, Shenyang 110142, China

³ Key Laboratory on Resources Chemicals and Material of Ministry of Education, Shenyang University Chemical Technology, Shenyang 110142, China

* Correspondence: iamwangna@syuct.com (N.W.); hongruiyao@syuct.edu.cn (H.Y.); Tel.: +86-024-89388092 (N.W. & H.Y.)

Received: 21 February 2020; Accepted: 20 March 2020; Published: 25 March 2020



Abstract: In this paper, graphene oxide (GO) was grafted with sodium tripolyphosphate (STP) to achieve a new anti-corrosive pigment (STG) with homogenous dispersion in waterborne epoxy (EP). The results obtained from Fourier transform infrared spectroscopy (FT-IR), X-ray photoelectron spectroscopy (XPS), transmission electron microscopy (TEM) and X-ray Diffraction (XRD) revealed that STP was successfully combined with GO by chemical bonding. The corrosion resistance of EP, GO/EP and STG/EP coatings on carbon steel substrates was investigated via electrochemical impedance spectroscopy (EIS) and salt spray test. The EIS results showed that the impedance value of coating with 0.7 wt.% STG reached $1.019 \times 10^9 \Omega \cdot \text{cm}^2$, which was considerably higher than that of neat waterborne EP coatings. Salt spray test results revealed once again that STG (0.7 wt.%)/EP coating had superior corrosion resistance. Besides, the STG (0.7 wt.%)/EP coated sample showed the highest adhesion strength between coating and substrate.

Keywords: waterborne epoxy; graphene oxide; corrosion; tripolyphosphate; coating

1. Introduction

The waterborne epoxy resin, a kind of thermosetting resin which has exceptional adhesion, anti-corrosion properties and characteristics of environmental friendliness, is frequently used in organic anti-corrosive coating [1,2]. However, some micro-holes and cracks will occur during the curing process of waterborne epoxy coating, which lead to reduction of coatings' anti-corrosive properties. One of the effective methods for improving the corrosion resistance of the waterborne epoxy coating is adding nano pigments, such as mesoporous materials [3–8], layered materials [9–11], metal-organic frameworks [12,13] and so on. In our previous work, ZSM-5 [14], mesoporous-TiO₂ [15,16], layered double hydroxides and metal-organic frameworks [17] have been investigated as anti-corrosive pigments. The results showed that porous and layered structure can improve the corrosion resistance of coatings via blocking or prolonging the erosion path of corrosive media, which was called the labyrinth effect.

Graphene, a promising two-dimensional (2D) carbon material, with excellent chemical stability and high barrier property, has been extensively applied in the field of epoxy anti-corrosive coating [18,19].

Nevertheless, the agglomeration of graphene caused by strong intersheet attractions (π - π stacking) severely restricts its practical application in waterborne epoxy coating. Surface modification or functionalization of graphene is a possible method to ensure effective dispersion of graphene in organic coatings and enhance the interfacial bonding between graphene and polymer matrix. In addition, many researches have reported that adding modified graphene or graphene oxide (GO) into epoxy coatings can significantly improve the anti-corrosive properties of coatings [7,8,20]. Yu et al. [20] prepared metronidazole grafted GO nanocomposites to enhance corrosion resistance of epoxy coating. Hu et al. [8] prepared nitrile functionalized graphene oxides composite coating to retard metal corrosion, via modified GO with the 3-aminophenoxyphthalonitrile. Chen et al. [7] prepared GO and phosphate (PO_4^{3-}) intercalated hydrotalcite via electrostatic self-assembly to realize improvement of anti-corrosive property of coatings.

Tripolyphosphate is a kind of amorphous water-soluble linear polyphosphate, which is often used as water retention agent, quality improver, dispersant and pH regulator in the food industry [21–24]. The metal can be protected by the passive film formed by the chelation of tripolyphosphate ions with metal ions [25]. Therefore, aluminum tripolyphosphate, sodium tripolyphosphate, calcium tripolyphosphate and zinc tripolyphosphate are all used in the field of anti-corrosion. Among them, sodium tripolyphosphate (STP) has the best water dispersibility, leading to a good application prospect in water-soluble polymers. It has been reported that functionalized graphite nanoplates and STP were combined to prepare anti-corrosive coatings, which promoted the anti-corrosive performance of the coating [26]. However, this promotion is restricted because above-mentioned two substances are bound by hydrogen bonds, which is very unstable and easy to be destroyed by external forces such as shear force.

In this paper, GO and STP were combined by chemical bonding to achieve a new kind of anti-corrosive pigment—graphene oxide grafted with sodium tripolyphosphate (STG). Then, the STG was added to a waterborne epoxy resin to improve its anti-corrosive performance and the protective mechanism of the composite coating was also discussed.

2. Materials and Methods

2.1. Materials

STP was purchased from Shanghai Mclean Biochemical Technology Co., Ltd. (Shanghai, China). Toluene was purchased from Tianjin Fuyu Fine Chemical Co., Ltd (Tianjin, China). KH-550 and methanol were provided by Tianjin Yongda Chemical Reagent Co., Ltd. (Tianjin, China). Epoxy resin and curing agent were purchased from Guangzhou Dai Xun commerce and Trade Co., Ltd. (Guangzhou, China). The GO was prepared by the modified Hummers' method reported in the previous work [27].

2.2. Methods

2.2.1. Amination of Sodium Tripolyphosphate (ASTP)

STP (4 g), toluene (50 mL), KH-550 (6 mL) were dissolved in beaker and poured into a three-neck flask which was equipped with stirrer. Then, the reaction system was kept at 70 °C and stirred continuously for 6 h. After the reaction, centrifuging the reaction solution with distilled water for 3–4 times and drying the reactants for later use.

2.2.2. Integration of Aminated Sodium Tripolyphosphate with Graphene Oxide

The integration of sodium tripolyphosphate with graphene oxide was carried out following the steps below. First, 0.04 g GO was dispersed in 40 mL distilled water and ultrasonicated for 30 min. Then, 20 mL EDC/NHS solution was added to the GO suspension. After activating for 30 min, 1 g ASTP was added to the mixed solution and stirred at 40 °C for 4 h. Finally, the reaction solution was washed with methanol for 3–4 times and dried in the drying oven. The STG was obtained for the following

experiments. Figure 1 gives a schematic diagram of the integration of sodium tripolyphosphate with graphene oxide.

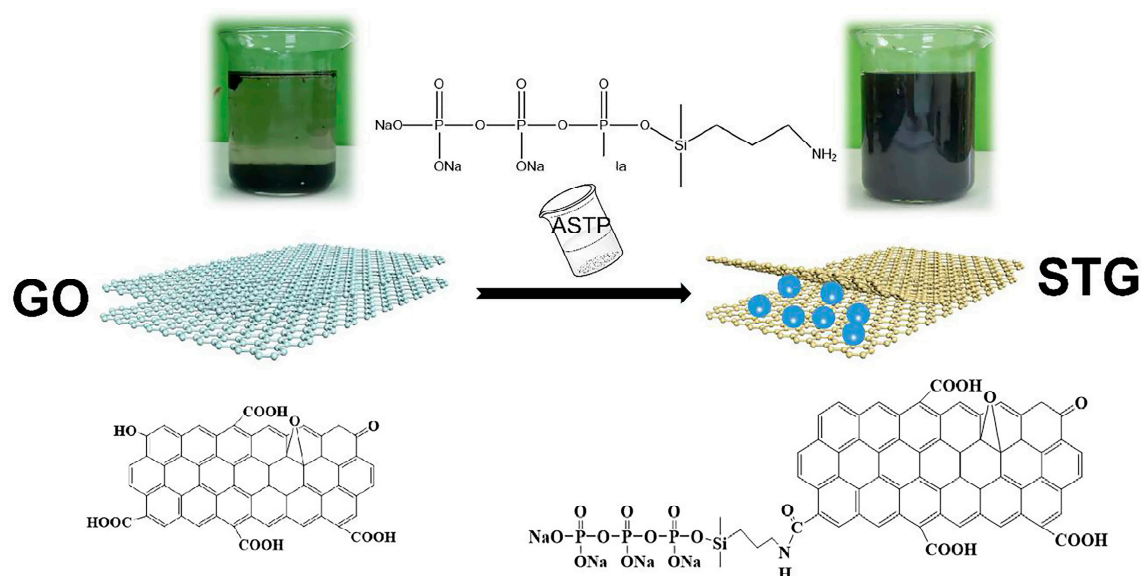


Figure 1. Schematic diagram of the integration of sodium tripolyphosphate with graphene oxide.

2.2.3. Preparation of the Composite Coating Modified by STG

To optimize the coating properties, composite coatings with different proportions (0.2 wt.%, 0.5 wt.%, 0.7 wt.%, 1.0 wt.%) of STG pigments were prepared. Besides, the neat epoxy coating and the composite coating with 0.7 wt.% GO pigment were also prepared for comparison (Table 1). The detailed preparation process was as follows:

Placing a certain amount of waterborne epoxy resin and STG pigment into a beaker. After fully stirring, weigh the corresponding quality of curing agent and deionize water into the mixture and stirred the mixture for 20 min to obtain the hybrid solution for further use. The steel substrates (Q235) were grounded to 150-grit SiC sandpaper and then ultrasonically cleaned in acetone for 15 min. Then, spraying the liquid paints onto the substrates by the compressed air sprayer and cured at room temperature. The coated samples were stored in dryer for one week before testing.

Table 1. Formulations of coatings.

Sample	Waterborne Epoxy Resin/g	Pigment/g	Curing Agent/g	Water/g
Neat epoxy	20	–	5	4
0.7 wt.% GO/EP	20	0.14	5	4
0.2 wt.% STG/EP	20	0.04	5	4
0.5 wt.% STG/EP	20	0.1	5	4
0.7 wt.% STG/EP	20	0.14	5	4
1.0 wt.% STG/EP	20	0.2	5	4

2.3. Characterization

Fourier transform infrared spectroscopy (FTIR) was used to characterize the chemical functionalities of GO, ASTP and STG. The spectra were recorded with a Nicolet Magna-IR560 (Artisan Technology Group, Austin, TX, USA) over the wave number range from 4000 to 400 cm^{-1} . X-ray Photoelectron Spectroscopy (XPS, ESCALAB MKLL electron spectrometer, VG Scientific, London, UK) was used to obtain the spectra of GO and STG. Diffraction patterns of GO and STG were recorded by X-ray diffraction (XRD, D/max-2500PC, Rigaku Corporation, Tokyo, Japan). The morphologies of samples were examined by transmission electron microscopy (TEM, JSM-6360LV, JEOL, Tokyo, Japan).

Anticorrosion tests of the composite coatings were conducted in 3.5 wt.% NaCl solution at room temperature. The electrochemical impedance spectroscopy (EIS) was measured by an electrochemical workstation (AUT84362, Autolab, Metrohm, Herisau, Switzerland) with the frequency ranged from 0.1 Hz to 100 kHz and the EIS data were analyzed by the ZSimpwin software (3.5, Metrohm, Shanghai, China).

The corrosion test of the coated specimens was performed by the neutral salt spray test. The condition used by the salt spray apparatus (YWα/Q-150) was specified by ASTM B117 [28], i.e., continuous spraying with 5.0 wt.% NaCl solution at 35 ± 2 °C. The surface of the test specimens was inspected, and the degree of rusting was rated by visual examination of the test specimens after 600 h.

The adhesion tests were conducted with PositestAT-M pull type automatic adhesion detector (Delelso, Ogdensburg, NY, USA) according to ASTM D4541-02 [29]. Six samples were selected from each group of samples for testing. The average values of the tests were the adhesion strength between coating and substrate.

3. Results

3.1. Characterization of STG

The FTIR spectra of GO, ASTP and STG are shown in Figure 2. The GO spectrum mainly showed four characteristic absorption peaks at 3423, 1732, 1628 and 1052 cm^{-1} , which were corresponded to $-\text{OH}$, $\text{C}=\text{O}$, $\text{C}=\text{C}$ and $\text{C}-\text{O}$ stretching vibration peaks, respectively [30]. The $\text{P}-\text{O}$ stretching vibration at 1168 cm^{-1} was the characteristic absorption peak of ASTP. Furthermore, the broad peak of $-\text{NH}$ at 3421 cm^{-1} and the absorption peak at 913 cm^{-1} prove the successful amination of STP [31]. For STG, the characteristic absorption peaks of both GO and ASTP can be observed in its infrared spectrum. In addition, the expansion vibration absorption peaks of $-\text{OH}$ and $-\text{NH}$ merged at 3412 cm^{-1} . Meanwhile, the absorption peaks of $-\text{CO}-\text{NH}-$ appeared at 1634 cm^{-1} in STG spectrum indicated that GO was successfully grafted with STP.

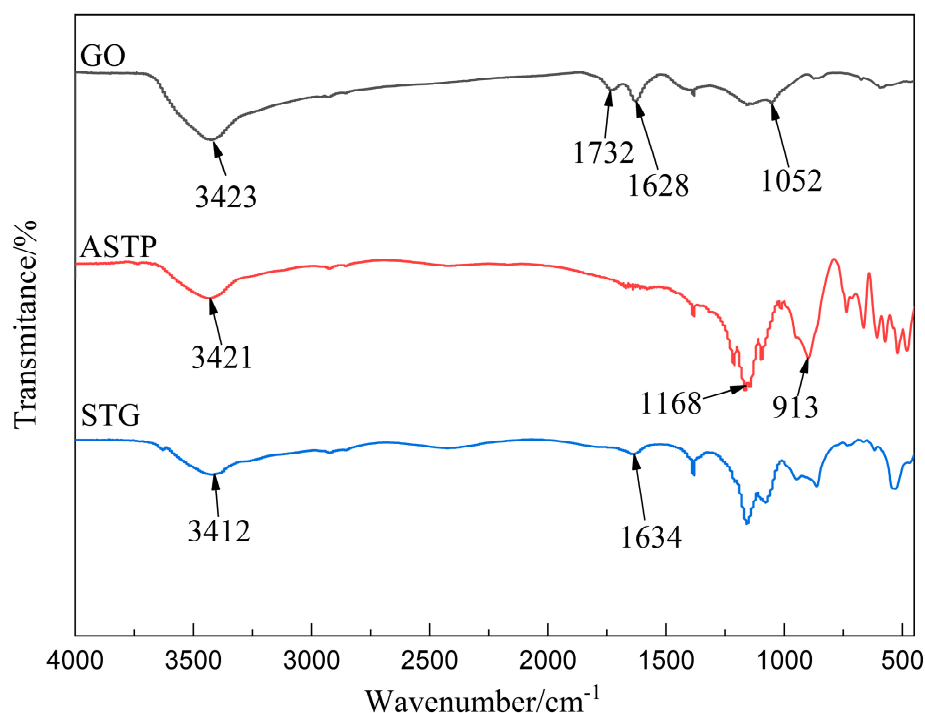


Figure 2. FTIR spectra of GO, ASTP and STG.

XPS characterization was used to further investigate the reaction between GO and ASTP, and the survey spectra are shown in Figure 3. The red line in Figure 3b–d represents the total fitting peak and the black line represents the raw peak. The full spectra in Figure 3a showed that the STG contained Na, O, C, P and Si, while the GO only contained C and O. Figure 3b–d shows the XPS spectra of C 1s, O 1s and Si 2p of STG respectively, which were fitted by the least square method using the Gaussian-Lorentzian envelope. Five binding energy features were obtained from the deconvolution curve fitting in the spectrum of C 1s (Figure 3b). The peak located at 289.2 eV was referred to O–C=O, and the remaining peaks centered at 286.1, 285.6, 284.9 and 284.4 eV were attributed to the C–N, C–OH, C–C and C=C, respectively. Figure 3c shows the binding energy spectrum of O 1s. The deconvolution of the O 1s gave six peaks located at 535.2, 532.7, 532.6, 531.9, 531.7 and 530.2 eV, which corresponded to phosphate group (PO_4^{3-}), –C=O, O–H, C–O, Si–O, N–C–O and Na–O, respectively. Compared with the C 1s and O 1s spectra of pure GO [32], the amide bond existed in the STG, which further confirmed the reaction between GO and ASTP. Besides, two peaks can be observed in the binding energy spectrum of Si 2p (Figure 3d). The first one at a binding energy of 102.8 eV was attributed to the Si–O and the second one appeared at 100.2 eV corresponded to Si–C, which revealed that Si was mainly connected with C and O atoms.

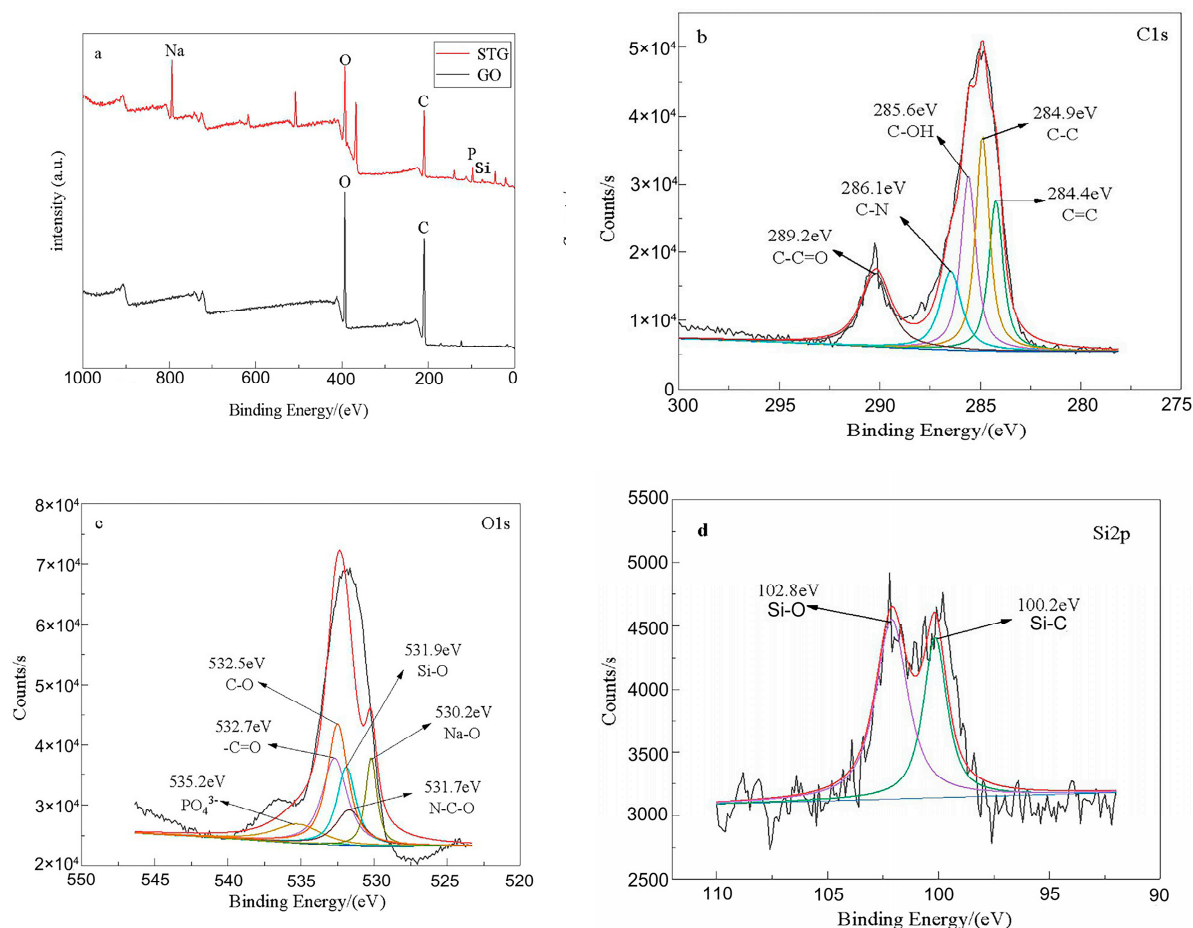


Figure 3. (a) XPS full spectra of GO and STG; (b) C 1s spectrum of STG; (c) O 1s spectrum of STG; (d) Si 2p spectrum of STG.

Figure 4 shows the images of GO and STG characterized by TEM. As shown in Figure 4a, pure GO was almost transparent under electron beam irradiation and there were obvious folds on the GO lamellae, which was because the GO had a super-thin structure [33]. After modification, dense and light spots appeared on GO surface as indicated by the red circles (Figure 4b), which indicated that the STP had successfully accessed to the GO surface.

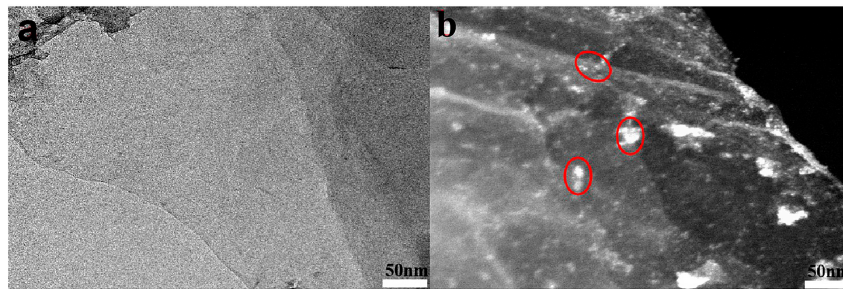


Figure 4. TEM images of (a) GO, (b) STG.

Figure 5 shows the XRD patterns of GO and STG. In Figure 5a, the diffraction peak of (002) plane of GO appeared at $2\theta = 9.4^\circ$, and the diffraction peak of (002) plane of STG appeared at $2\theta = 8.3^\circ$. It could be calculated that the interlamellar spacing (d-spacing) of GO was 0.939 nm and the interlamellar spacing of STG was 1.070 nm, according to the Bragg calculator. This indicated STG was successfully inserted into the interlamellar of GO, combined with the TEM images.

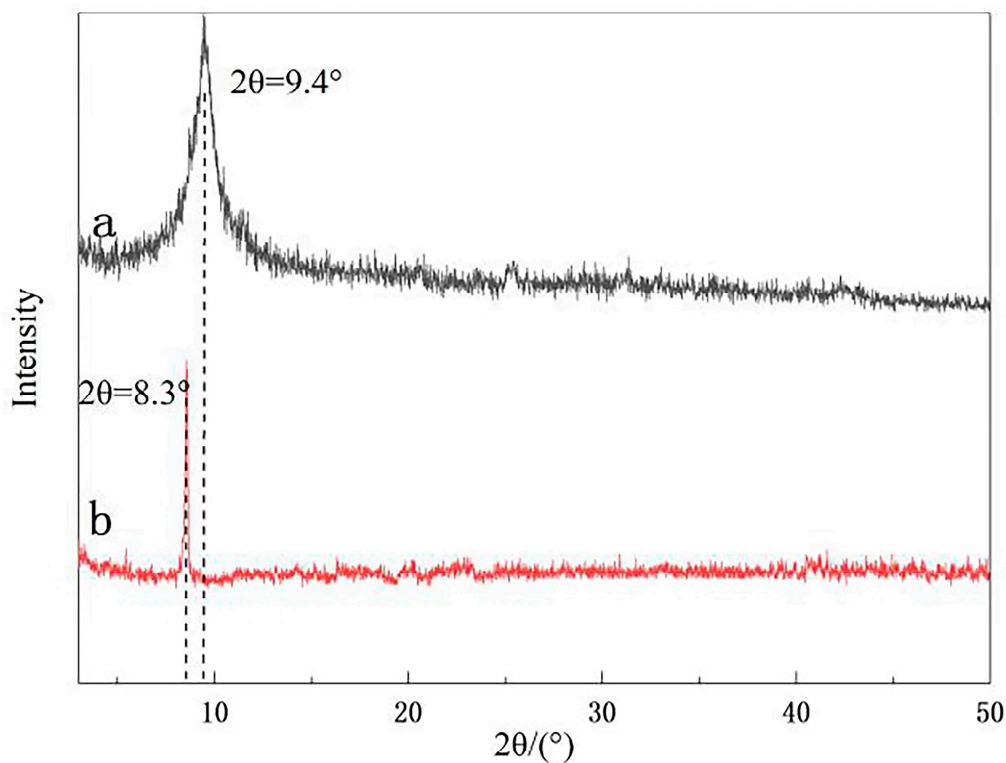


Figure 5. XRD patterns of (a) GO, (b) STG.

3.2. Characterization of the Composite Coatings

EIS is an effective technique to evaluate and predict the barrier and corrosion resistance of organic coatings [33,34]. Figure 6 shows the Nyquist and Bode plots of coatings at different immersion times in 3.5 wt.% NaCl solution. It has been generally accepted that the larger the radius of the impedance arc, the better corrosion protective performance [35].

As observed from Figure 6a, GO/EP and STG/EP coatings had larger radius of impedance arcs than neat EP coating in the initial immersion, confirming the barrier effect of composite coatings had been remarkably enhanced by adding anti-corrosive pigments, especially the STG pigment. The impedance modulus at the lowest frequency ($Z_f = 0.1$ Hz) in Bode plot could be used as a semi-quantitative indicator of coating's corrosion resistance. The $Z_f = 0.1$ Hz values of experimental coatings are in

order: STG (0.7 wt.)/EP > STG (1.0 wt.)/EP > STG (0.5 wt.)/EP > STG (0.2 wt.)/EP > GO/EP > EP (Figure 6d). Among them, the $Z_f = 0.1$ Hz values of STG (0.7 wt.)/EP coating ($1.019 \times 10^9 \Omega \cdot \text{cm}^2$) was two orders of magnitude higher than that of neat EP coating ($2.657 \times 10^7 \Omega \cdot \text{cm}^2$), which was consistent with the Nyquist plot results. Besides, it could also be seen that the $Z_f = 0.1$ Hz values increased first and then decreased with the increase of STG pigment amount, which was because only appropriate amount pigment can improve the corrosion resistance of EP coatings. Low addition of pigment was not sufficient to make up for the defect of EP, while the excess addition might cause pigment to aggregate in EP, resulting in new defects and then decreasing coating's corrosion resistance, such as STG (1.0 wt.)/EP coating. In this stage, the Nyquist curve can be fitted with the equivalent circuit showed in Figure 7a, which contains the solution resistance (R_s), the coating capacitance (C_c) and the pore resistance (R_{po}).

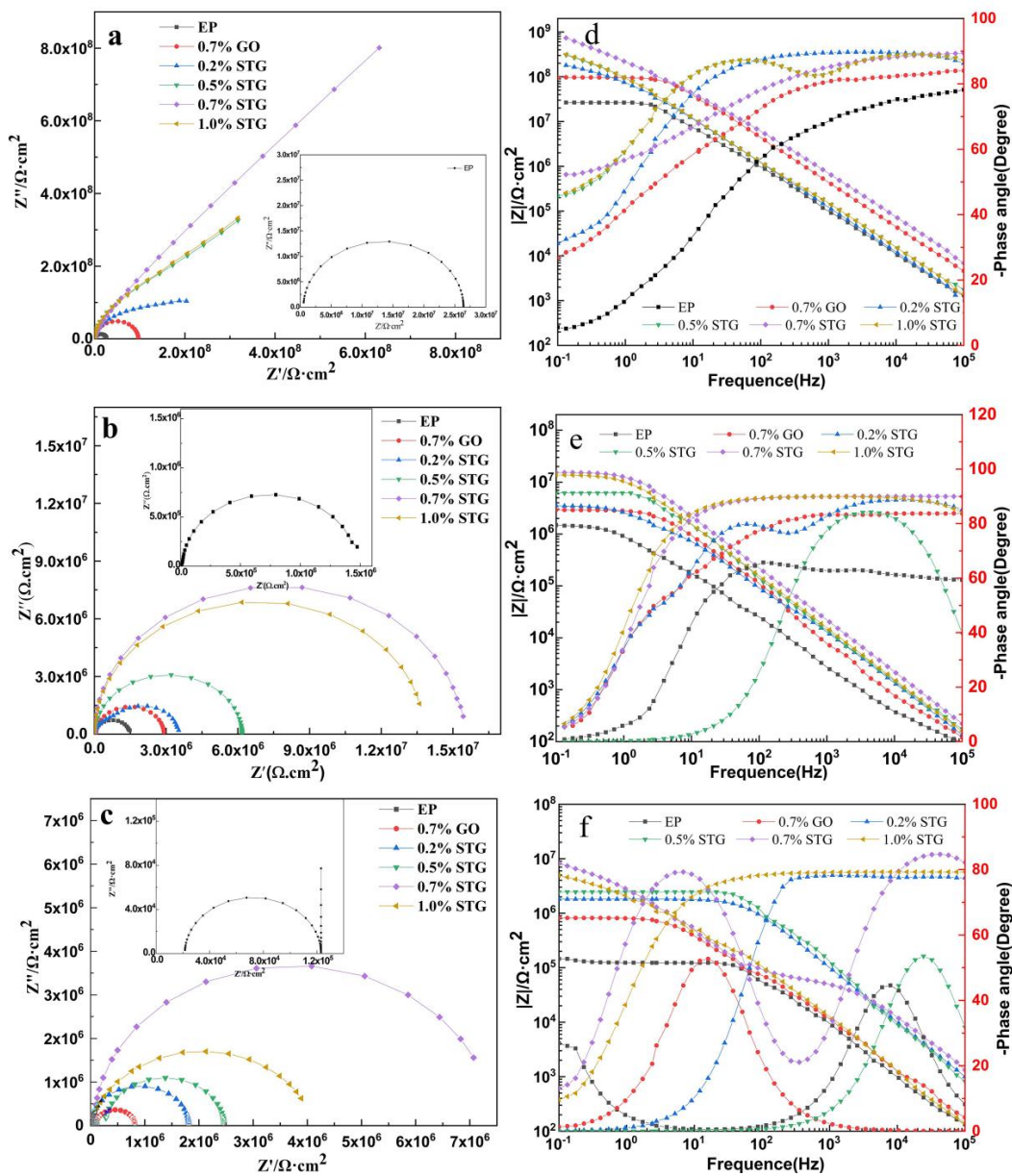


Figure 6. The Nyquist and Bode plots of different samples after 2 h (a-Nyquist, d-Bode), 360 h (b-Nyquist, e-Bode) and 720 h (c-Nyquist, f-Bode) immersion in 3.5 wt.% NaCl solution.

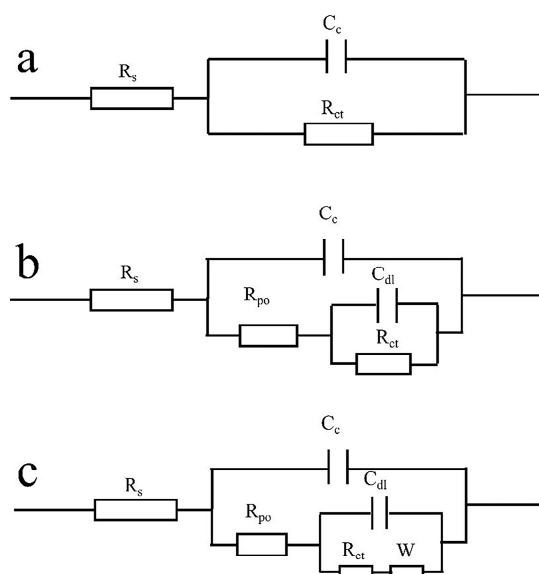


Figure 7. Equivalent electrical circuits models.

After 360 h immersion, an obvious capacitance arc appeared in Figure 6b and the $Z_f = 0.1$ Hz values all coatings was obviously decreased in Figure 6e, because of the absorption of corrosive medium and the creation of transport pathways to the substrate through the defects or pores. The $Z_f = 0.1$ Hz values of neat EP coating and STG (0.7 wt.)/EP coating declined to $1.488 \times 10^6 \Omega$ and $1.528 \times 10^7 \Omega \cdot \text{cm}^2$, respectively, which indicated that the protective capacity of coatings began to degenerate gradually. At this point, the phase angle in Bode plots shows that the coatings exhibited a two-time constant behavior after 360 h exposure, and the equivalent circuit diagram conforms to Figure 7b, where C_{dl} and R_{ct} represents the double layer capacitance of foaming part and the charge transfer resistance (R_{ct}), respectively.

The Nyquist diagram of coatings after 720 h immersion is shown in Figure 6c. A diffusion field at low frequencies appeared around the neat EP coated sample, which indicated that corrosion products began to accumulate on the steel surface and penetrated into the neat EP coating gradually. At this stage, the equivalent circuit showed in Figure 7c included Warburg impedance element (W) was applicable to the neat EP coatings. Figure 6f shows that the $Z_f = 0.1$ Hz values of all coatings continued to decline. The $Z_f = 0.1$ Hz value of GO/EP coating had reduced to $8.206 \times 10^5 \Omega \cdot \text{cm}^2$, however, the $Z_f = 0.1$ Hz value of STG/EP coating was close to $1 \times 10^7 \Omega \cdot \text{cm}^2$. This could be attributed to corrosive inhibition by the released phosphate ions from STG. The equivalent circuit showed in Figure 7b was still applicable to the composite coatings.

Equivalent circuits:

$$\text{Model 1: } R_p = 1/R_{ct} \tag{1}$$

$$\text{Model 2: } R_p = R_{po} \times R_{ct}/(R_{po} + R_{ct}) \tag{2}$$

$$\text{Model 3: } R_p = R_{po} \times R_{ct}/(R_{po} + R_{ct}) \tag{3}$$

The fitting parameters of neat EP, GO (0.7 wt.)/EP and STG (0.7 wt.)/EP coatings at different soaking stages are shown in Table 2. In order to compare the corrosion resistance of coatings, the polarization resistance (R_p) has been calculated with models 1–3, which can reflect the anti-corrosive performance of the coatings to some extent [36,37]. Figure 8 shows the calculated R_p of the experimental coatings immersed in 3.5 wt.% NaCl solution for 2, 360 and 720 h. Initially, the maximum R_p value of STG (0.7 wt.)/EP coatings was $7.731 \times 10^8 \Omega \cdot \text{cm}^2$, while the R_p values of pure EP and GO/EP coatings were 5.589×10^7 and $9.629 \times 10^7 \Omega \cdot \text{cm}^2$, respectively. The trend remained stable with the immersion time increases. Although the R_p value of all coatings decreased after immersion, the composite coatings with STG pigment still had the better corrosion resistance than neat EP and GO/EP

coatings. For example, after immersing for 360 h, the R_p value of STG (0.7 wt.%)/EP coating was $6.432 \times 10^7 \Omega \cdot \text{cm}^2$, which was higher than that of neat EP coating ($9.913 \times 10^5 \Omega \cdot \text{cm}^2$).

Table 2. The parameters of the fitting circuit.

Sample	Time (h)	R_s ($\Omega \cdot \text{cm}^2$)	C_c ($\text{F} \cdot \text{cm}^{-2}$)	R_{ct} ($\Omega \cdot \text{cm}^2$)	R_{po} ($\Omega \cdot \text{cm}^2$)	C_{dl} ($\text{F} \cdot \text{cm}^{-2}$)	W ($\Omega \cdot \text{cm}^2$)
EP	2	5.165×10^5	2.971×10^{-12}	5.589×10^7	–	–	–
	360	6.392×10^4	2.171×10^{-11}	2.846×10^6	3.594×10^8	7.402×10^{-8}	–
	720	2.138×10^4	5.064×10^{-10}	1.032×10^6	7.281×10^5	1.556×10^{-5}	3.104×10^{-10}
0.7 wt.% GO/EP	2	5.826×10^4	2.754×10^{-10}	9.629×10^7	–	–	–
	360	6.507×10^4	1.647×10^{-9}	2.846×10^6	3.594×10^8	2.225×10^{-15}	–
	720	9.278×10^4	4.265×10^{-8}	1.032×10^6	7.281×10^5	5.581×10^{-12}	4.085×10^{-12}
0.7 wt.% STG/EP	2	1.652×10^5	2.557×10^{-10}	7.731×10^8	–	–	–
	360	5.567×10^4	7.179×10^{-9}	3.135×10^7	1.156×10^8	1.935×10^{-12}	–
	720	1.887×10^4	1.216×10^{-9}	1.812×10^6	2.197×10^6	3.506×10^{-8}	–

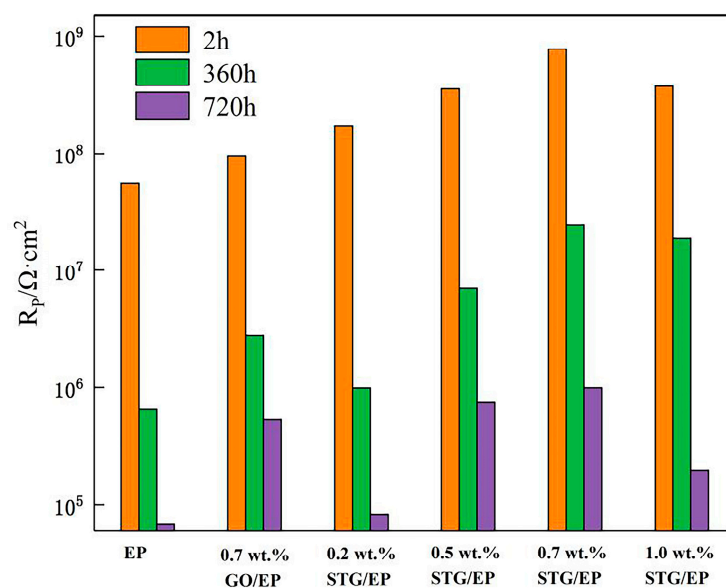


Figure 8. Polarization resistance of the three coatings at immersion times of 2, 360, 720 h in 3.5 wt.% NaCl solution.

To further observe the anti-corrosive performance of composite coatings, the salt spray test was carried out. The surface morphologies of all coatings after 600 h salt spray test are shown in Figure 9. Comparing the six Figures (Figure 9a–f), it could be found that all the coatings had different degrees of corrosion. The neat EP coating in Figure 9a showed obvious rust the most, which presented that the composite coatings modified by pigments could effectively prevent corrosion ions and enhanced the corrosion resistance of the coatings. Moreover, the composite coatings modified by STG had better corrosion resistance than GO/EP, which indicated that the improvement of nano-pigments' water solubility could improve the corrosion resistance of coating. The anti-corrosive performance of coatings with STG increased firstly and then decreased with the increase of STG amount, which was in accordance with the EIS results. There was no obvious rust spot on the surface of STG (0.7 wt.%)/EP coating (Figure 9e), which illustrated that the waterborne EP coating modified by 0.7 wt.% STG pigment had the best corrosion resistance.

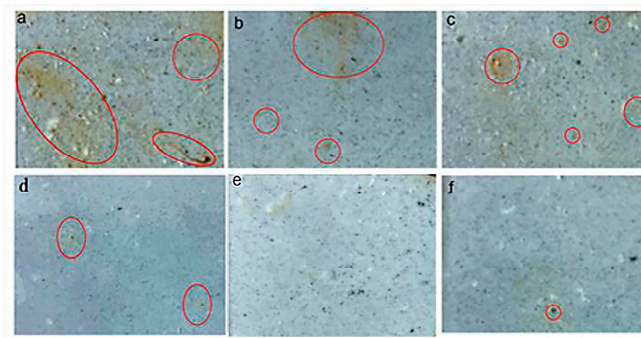


Figure 9. Surface morphologies of the coatings after the salt spray test for 600 h: (a) neat EP; (b) GO (0.7 wt.)/EP; (c) STG (0.2 wt.)/EP; (d) STG (0.5 wt.)/EP; (e) STG (0.7 wt.)/EP; and (f) STG (1.0 wt.)/EP.

Figure 10 represents adhesion test charts of all samples. It could be seen from the Figure 10 that the adhesion strength of composite coatings was greater than that of neat EP coatings without pigments. This was ascribed that the addition of pigments enhanced the force between composite coating and metal matrix. For GO (0.7 wt.)/EP coating, the adhesion strength improved from 7.32 to 8.63 MPa. Compared with GO/EP coating, STG/EP coatings represented stronger adhesion strength. The maximum adhesion strength reached to 11.65 MPa. This phenomenon was caused by the improvement of pigments' water solubility, which made the pigment better fill the defects in the coatings to improve coating's adhesion strength. For the STG/EP coatings, the values of adhesion first increased and then decreased with the increase of STG amount. This trend was as same as the result of EIS, which was because of the new defects' formation caused by the excessive pigment's amount.

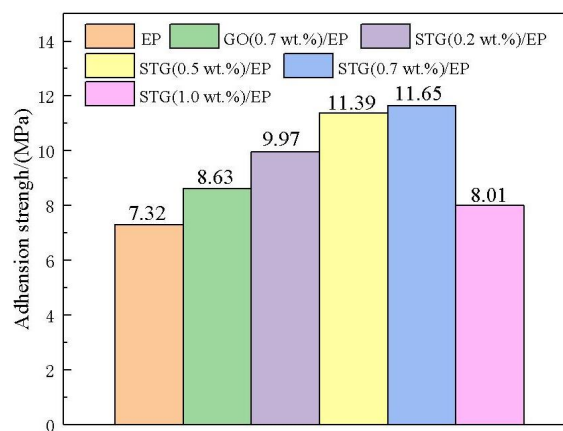


Figure 10. Diagram of coatings adhesion test.

4. Conclusions

GO and STP were combined by chemical bonding and then STG was obtained. STG was characterized by FT-IR, TEM, XPS, XRD. The results proved that STG was successfully synthesized by inserting STP into GO layers, and the water solubility of STG was obviously better than that of GO. The corrosion resistance of coatings was investigated by EIS and salt spray test. The results were as follows:

- The result of EIS showed that both GO and STG could obviously improve the anti-corrosive properties of waterborne EP coating and lengthen protection time. Compared with GO/EP coating, the STG/EP coatings had better corrosion resistance with same addition amount.
- The result of salt spray test showed the rust on the surface of waterborne EP coatings decreased after adding GO or STG. Moreover, the rust first decreased and then increased with increase in

the amount of STG pigment, and the 0.7 wt.% STG/EP coating showed best corrosion resistance compared with other coatings.

Author Contributions: Conceptualization, N.W. and X.Y.; Data curation, X.Y., H.G. and X.D.; Formal analysis, N.W. and X.Y.; Funding acquisition, N.W.; Investigation, X.Y.; Methodology, H.G., X.D. and J.Z.; Project administration, N.W.; Resources, N.W. and X.Y.; Writing—Original draft, N.W. and X.Y.; Writing—Review and editing, N.W., H.Y. and X.Y. All authors have read and agreed to the published version of the manuscript.

Funding: This research was funded by the financial support for her research group by the National Natural Science Foundation of China, grant number No.51973124; National Key R&D Program “Science and Technology Winter Olympics”, grant number No.2019YFF0302004; Sino-Spanish Advanced Materials Institute, Shenyang Municipal Science and Technology Bureau, grant number No.18-005-6-04; Department of Science & Technology of Liaoning province-Shenyang National Laboratory for Materials Science Joint R & D Fund Project, grant number No. 2019JH3/30100015.

Conflicts of Interest: The authors declare no conflict of interest.

References

1. Tang, G.W.; Ren, T.T.; Yan, Z.S. Corrosion resistance of a self-curing waterborne epoxy resin coating. *J. Coat. Technol. Res.* **2019**, *16*, 895–904. [[CrossRef](#)]
2. Yuan, C.; Zhao, M.; Sun, D.; Guo, R. Preparation and properties of few-layer graphene modified waterborne epoxy coatings. *J. Appl. Polym. Sci.* **2018**, *135*, 41. [[CrossRef](#)]
3. Wang, H.; Gan, M.; Ma, L.; Zhou, T. Synthesis of polyaniline-modified mesoporous-silica containers for anticorrosion coatings via in-situ polymerization and surface-protected etching. *Polym. Adv. Technol.* **2016**, *27*, 929–937. [[CrossRef](#)]
4. Alipour, K.; Nasirpouri, F. Smart anti-corrosion self-healing zinc metal-based molybdate functionalized-mesoporous-silica (MCM-41) nanocomposite coatings. *RSC Adv.* **2017**, *7*, 51879–51887. [[CrossRef](#)]
5. Borisova, D.; MoHwald, H.; Shchukin, D.G. Mesoporous silica nanoparticles for active corrosion protection. *ACS Nano* **2011**, *5*, 1939–1946. [[CrossRef](#)] [[PubMed](#)]
6. Wang, N.; Fu, W.; Sun, M. Effect of different structured TiO₂ particle on anticorrosion properties of waterborne epoxy coatings. *Corros. Eng. Sci. Technol.* **2016**, *51*, 365–372. [[CrossRef](#)]
7. Chen, C.; He, Y.; Xiao, G. Synergistic effect of graphene oxide@phosphate-intercalated hydrotalcite for improved anti-corrosion and self-healable protection of waterborne epoxy coating in salt environments. *J. Mater. Chem. C* **2019**, *7*, 2318–2326. [[CrossRef](#)]
8. Hu, H.; He, Y.; Long, Z. Synergistic effect of functional carbon nanotubes and graphene oxide on the anti-corrosion performance of epoxy coating. *Polym. Adv. Technol.* **2017**, *28*, 754–762. [[CrossRef](#)]
9. Liu, S.; Gu, L.; Zhao, H.; Chen, J.; Yu, H. Corrosion resistance of graphene-reinforced waterborne epoxy coatings. *J. Mater. Sci. Technol.* **2016**, *32*, 425–431. [[CrossRef](#)]
10. Tian, Y.; Xie, Y.; Dai, F.; Huang, H.; Zhong, L.; Zhang, X. Ammonium-grafted graphene oxide for enhanced corrosion resistance of waterborne epoxy coatings. *Surf. Coat Technol.* **2020**, *383*, 125227.
11. Cui, M.; Ren, S.; Chen, J.; Liu, S.; Zhang, G.; Zhao, H. Anti-corrosive performance of waterborne epoxy coatings containing water-dispersible hexagonal boron nitride (h-BN) nanosheets. *Appl. Surf. Sci.* **2017**, *397*, 77–86. [[CrossRef](#)]
12. Mesbah, A.; Jacques, S.; Rocca, E.; François, M.; Steinmetz, J. Compact Metal–Organic Frameworks for Anti-Corrosion Applications: New Binary Linear Saturated Carboxylates of Zinc. *Eur. J. Inorg. Chem.* **2011**, *8*, 1315–1321. [[CrossRef](#)]
13. Zhang, M.; Ma, L.; Wang, L. Insights into the use of metal-organic framework as high performance anti-corrosion coatings. *ACS Appl. Mater. Interfaces* **2018**, *10*, 2259–2263. [[CrossRef](#)] [[PubMed](#)]
14. Wang, N.; Gao, H.; Zhang, J. Effect of graphene oxide/ZSM-5 hybrid on corrosion resistance of waterborne epoxy coating. *Coatings* **2018**, *8*, 179. [[CrossRef](#)]
15. Wang, N.; Fu, W.; Zhang, J. Corrosion performance of waterborne epoxy coatings containing polyethylenimine treated mesoporous-TiO₂ nanoparticles on mild steel. *Prog. Org. Coat.* **2015**, *89*, 114–122. [[CrossRef](#)]
16. Wang, N.; Diao, X.; Zhang, J. Corrosion resistance of waterborne epoxy coatings by incorporation of dopamine treated mesoporous-TiO₂ particles. *Coatings* **2018**, *8*, 209. [[CrossRef](#)]

17. Wang, N.; Zhang, Y.; Chen, J. Dopamine modified metal-organic frameworks on anti-corrosion properties of waterborne epoxy coatings. *Prog. Org. Coat.* **2017**, *109*, 126–134. [[CrossRef](#)]
18. Kirkland, N.T.; Schiller, T.; Medhekar, N. Exploring graphene as a corrosion protection barrier. *Corros. Sci.* **2012**, *56*, 1–4. [[CrossRef](#)]
19. Liu, J.; Liu, T.; Guo, Z. Promoting barrier performance and cathodic protection of zinc-rich epoxy primer via single-layer graphene. *Polymers* **2018**, *10*, 591. [[CrossRef](#)]
20. Yu, Z.; Lv, L.; Ma, Y. Covalent modification of graphene oxide by metronidazole for reinforced anti-corrosion properties of epoxy coatings. *RSC Adv.* **2016**, *6*, 18217–18226. [[CrossRef](#)]
21. Lim, H.M.; Yang, H.C.; Chun, B.S. The effect of sodium tripolyphosphate on sodium silicate-cement grout. *Mater. Sci. Forum.* **2005**, *486*, 391–394. [[CrossRef](#)]
22. Krause, R.J.; Ockerman, H.W.; Krol, B. Influence of tumbling, tumbling time, trim and sodium tripolyphosphate on quality and yield of cured hams. *J. Food. Sci.* **1978**, *43*, 853–855. [[CrossRef](#)]
23. Young, L.L.; Lyon, B.G. Effect of sodium tripolyphosphate in the presence and absence of calcium chloride and sodium chloride on water retention properties and shear resistance of chicken breast meat. *Poult. Sci.* **1986**, *65*, 898–902. [[CrossRef](#)]
24. Liu, D.; Zhao, C.; Guo, M. Sodium tripolyphosphate inhibits the formation of lysinoalanine in heat-treated whey protein. *J. Food. Process. Preserv.* **2017**, *41*, e13501. [[CrossRef](#)]
25. Engström, B.; Nordberg, G.F. Effects of detergent formula chelating agents on the metabolism and toxicity of cadmium in mice, Basic. *Clin. Pharmacol.* **2010**, *43*, 387–397.
26. Mohammadi, S.; Shariatpanahi, H.; Taromi, F.A. Electrochemical and anticorrosion behaviors of hybrid functionalized graphite nano-platelets/tripolyphosphate in epoxy-coated carbon steel. *Mater. Res. Bull.* **2016**, *80*, 7–22. [[CrossRef](#)]
27. Xian, H.Y.; Peng, T.J.; Sun, H.J. Effect of particle size of natural flake graphite on the size and structure of graphene oxide prepared by the modified hummers method. *Mater. Sci. Forum.* **2015**, *814*, 185–190. [[CrossRef](#)]
28. ASTM B117-03 Standard Practice for Operating Salt Spray (Fog) Apparatus; ASTM International: West Conshohocken, PA, USA, 2003.
29. ASTM D4541-02 Standard Test Method for Pull-off Strength of Coatings Using Portable Adhesion Testers; ASTM International: West Conshohocken, PA, USA, 2002.
30. Vlasceanu, G.M.; Crica, L.E.; Pandele, A.M.; Ionita, M. Graphene oxide reinforcing genipin crosslinked chitosan-gelatin blend films. *Coatings* **2020**, *10*, 189. [[CrossRef](#)]
31. Ma, X.H.; Xu, Z.L.; Ji, C.Q.; Wei, Y.M.; Yang, H. Characterization, separation performance, and model analysis of stpp-chitosan/pan polyelectrolyte complex membranes. *J. Appl. Polym. Sci.* **2011**, *120*, 1017–1026. [[CrossRef](#)]
32. Li, Z.; González, A.J.; Heeralal, V.B. Covalent assembly of MCM-41 nanospheres on graphene oxide for improving fire retardancy and mechanical property of epoxy resin. *Compos. Part B* **2018**, *138*, 101–112. [[CrossRef](#)]
33. Niknahad, M.; Moradian, S.; Mirabedini, S.M. The adhesion properties and corrosion performance of differently pretreated epoxy coatings on an aluminium alloy. *Corros. Sci.* **2010**, *52*, 1948–1957. [[CrossRef](#)]
34. Ma, Y.; Fan, B.; Zhou, T. Molecular assembly between weak crosslinking cyclodextrin polymer and trans-cinnamaldehyde for corrosion inhibition towards mild steel in 3.5% NaCl solution: Experimental and theoretical studies. *Polymers* **2019**, *11*, 635. [[CrossRef](#)] [[PubMed](#)]
35. Yanning, C.; Baohui, R.; Shuiying, G.; Rong, C. The sandwich-like structures of polydopamine and 8-hydroxyquinoline coated graphene oxide for excellent corrosion resistance of epoxy coatings. *J. Colloid Interface Sci.* **2020**, *565*, 436–448.
36. Fan, F.; Zhou, C.; Wang, X. Layer-by-layer assembly of a self-healing anticorrosion coating on magnesium alloys. *ACS Appl. Mater. Interfaces* **2015**, *7*, 27271–27278. [[CrossRef](#)] [[PubMed](#)]
37. Das, M.; Biswas, A.; Kumar, B.K. Enhanced pseudo-halide promoted corrosion inhibition by biologically active zinc(ii) schiff base complexes. *Chem. Eng. J.* **2019**, *357*, 447–457. [[CrossRef](#)]

